HHS Public Access

Author manuscript

Magn Reson Med. Author manuscript; available in PMC 2020 December 01.

Published in final edited form as:

Magn Reson Med. 2019 December ; 82(6): 2248–2256. doi:10.1002/mrm.27888.

Non-invasive Imaging of Oxygen Concentration in a Complex *In Vitro* Biofilm Infection Model Using ^{19}F MRI: Persistence of an Oxygen Sink Despite Prolonged Antibiotic Therapy

Jeffrey W. Simkins[1,2], **Philip S. Stewart**[1,2], **Sarah L. Codd**[1,3], **Joseph D. Seymour**[1,2,*]

[1]Center for Biofilm Engineering, Montana State University, Bozeman MT USA 59715-3920

[2]Department of Chemical and Biological Engineering, Montana State University, Bozeman MT USA 59715-3920

[3]Department of Mechanical and Industrial Engineering, Montana State University, Bozeman MT USA 59715-3920

Abstract

Purpose: Oxygen availability is a critical determinant of microbial biofilm activity and antibiotic susceptibility. However, measuring oxygen gradients in these systems remains difficult, with the standard microelectrode approach being both invasive and limited to single-point measurement. The goal of the study was to develop a ^{19}F Magnetic Resonance Imaging approach for two-dimensional oxygen mapping in biofilm systems and to visualize oxygen consumption behavior in real time during antibiotic therapy.

Methods: Oxygen-sensing beads were created by encapsulating an emulsion of oxygen-sensing fluorocarbon into alginate gel. *Escherichia coli* biofilms were grown in and on the alginate matrix which was contained inside a packed bed column subjected to nutrient flow, mimicking the complex porous structure of human wound tissue, and subjected to antibiotic challenge.

Results: The linear relationship between ^{19}F spin-lattice relaxation rate R_1 and local oxygen concentration permitted noninvasive spatial mapping of oxygen distribution in real-time over the course of biofilm growth and subsequent antibiotic challenge. This technique was used to visualize persistence of microbial oxygen respiration during continuous gentamicin administration, providing a time series of complete spatial maps detailing the continued bacterial utilization of oxygen during prolonged chemotherapy in an *in vitro* biofilm model with complex spatial structure.

Conclusions: Antibiotic exposure temporarily causes oxygen consumption to enter a pseudo-steady state wherein oxygen distribution becomes fixed; oxygen sink expansion resumes quickly after antibiotic clearance. This technique may provide valuable information for future investigations of biofilms by permitting the study of complex geometries (typical of *in vivo* biofilms) and facilitating noninvasive oxygen measurement.

[*]Corresponding author: Joseph D. Seymour, jseymour@montana.edu, 1-406-994-6853, 306 Cobleigh Hall, Chemical and Biological Engineering, Montana State University, Bozeman MT 59715-3920.

Keywords

Oximetry; Biofilms; Antibiotics; Infection Persistence; MRI

1. INTRODUCTION

Molecular oxygen plays a profound role in biofilm presentation (1), shaping microbial diversity (2), gene expression and metabolism (3), and in the case of medical biofilms, infection persistence (4). Gradients in oxygen concentration arise in biofilm systems through the simultaneous reaction and diffusion of this electron acceptor (5). Oxygen utilization by active bacterial and host cells generates anoxic zones (6–8), inducing bacteria contained therein to transition to a state of dormancy which imparts tolerance to antimicrobials (9; 10) and host immune defenses (11). As a consequence, oxygen penetration into infected tissue is a strong predictor of clinical outcome (12), and therapies stimulating oxygen delivery into colonized wounds have proven effective (13). However, despite the importance of oxygen in medical biofilms, mapping oxygen concentration in these systems remains a cumbersome endeavor, with the traditional microelectrode approach being both invasive and limited to single-point measurement (14).

The spin-lattice relaxation rate R_1 of ^{19}F nuclei in perfluorocarbons (PFCs) is linearly proportional to local oxygen concentration (15). This relationship has been exploited in the biomedical literature to measure pO_2 in blood (16), tissues (17), and tumors (18). To facilitate oxygen mapping in a biofilm system, we encapsulated an emulsion containing an oxygen-sensing PFC, perfluorooctylbromide (PFOB), into alginate gel beads such that PFC is both fixed and evenly distributed throughout the experiment. Encapsulation of PFC in alginate beads to facilitate long-term immobilization in tissues has been previously described by Nöth et al. (19), and PFOB in particular has proved to be an attractive oximetry option due to its stability in aqueous emulsions, and has been used to measure oxygen in a variety of biological tissues (20–23). Bacterial growth is initiated in the PFC-laden alginate beads by inoculating the emulsion before gel solidification (24). As bacterial growth inside an alginate gel matrix is frequently used as an *in vitro* biofilm model, this approach allows for the noninvasive mapping of oxygen inside a conventional and well-studied biofilm system with *in vivo* relevance (25–29). Gel beads, one inoculated and the others sterile, are packed into a chromatography column and nutrient media is fed into the column at a volumetric flowrate of 25 mL/h, yielding a complex porous medium containing liquid flow amidst tissue-like occlusions, which better approximates the growth conditions of real *in vivo* biofilms than planar biofilm models and may thus better capture their behavior.

The objective of the present study was to utilize these novel oxygen-sensing alginate beads to facilitate noninvasive, two-dimensional spatial mapping of oxygen profile in a clinically-relevant biofilm system undergoing chemical challenge by a broad-spectrum antibiotic. Successful application of this technique would exhibit distinct advantages over conventional approaches, namely the ability to visualize oxygen distribution in multiple dimensions, the ability to quantify oxygenation in biofilm systems characterized by complex geometry (similar to real biofilms encountered in medicine), and the ability to measure transient

responses to changes in chemical environment due to the lack of invasiveness and simultaneous sample-wide signal acquisition.

2. METHODS

2.1 Bacterial cultivation

The bacterium used in these experiments was an *Escherichia coli* (*E. coli*) HB101 strain containing plasmid pMF440 (provided by Dr. Michael Franklin; Addgene plasmid #62550), conferring constitutive expression of red fluorescent protein (RFP) recombinant mCherry, in addition to an ampicillin resistance gene. Inocula were cultured overnight at 37 ºC in a shaking incubator with full-strength tryptic soy broth (TSB) and 100 μg/mL ampicillin to promote retention of the plasmid. To demonstrate the efficacy of gentamicin against planktonic cells, a subset overnight cultures were grown in the presence of 50 μg/mL GEN. No growth was observed (data not shown).

2.2 Oxygen-sensing alginate beads

All glassware and the shear mixer downshaft were autoclaved prior to alginate bead creation, and all steps in the protocol were conducted in a sterile biological safety cabinet under laminar airflow to prevent contamination by ambient microbes. Perfluorooctylbromide (PFOB) was selected as the oxygen-sensing PFC as it readily forms stable emulsions in water. ^{19}F oxygen-sensing alginate gel beads were created by dissolving 0.4 g α-phosphatidylcholine surfactant (Sigma; P3556) and 0.2 g low-viscosity sodium alginate (Sigma; A1112) in 10 mL of deionized water. 9g PFOB (Aurum Pharmatech; K-8801) was introduced into the beaker and the solution was homogenized at 15,000 rpm for 30 minutes with a shear mixer to generate a 90% w/v emulsion of a PFOB in an aqueous solution containing 2% w/v sodium alginate. The emulsion was divided into two aliquots, with the first aliquot then dripped into a 50 mM solution of calcium chloride (Sigma; C1016) with a burette. The dripping process generated spherical alginate beads with an average diameter of 3.42 ± 0.23 mm containing dispersed PFC. A 1 mL aliquot of the overnight culture was centrifuged at 6,000 rpm for 4 minutes, resuspended in sterile phosphate-buffered saline, and used to inoculate the second emulsion aliquot at a final dilution of 1:10,000. The inoculated emulsion aliquot was then dripped into the calcium chloride bath to generate beads containing the oxygen-sensing PFC as well as gel-entrapped bacterial colonies, a common *in vitro* biofilm model (25–27).

2.3 pO_2 vs R_1 calibration curve for PFOB

Nuclear Magnetic Resonance (NMR) calibration experiments were conducted as described previously (24). All experiments were performed on a 7 T vertical-bore magnet with an actively shielded micro2.5 gradient probe providing 1.5 T/m at 60 A, under the control of a Bruker Avance III MRI spectrometer. To construct a calibration curve for the R_1 of PFOB as a function of pO_2 in the anoxic to atmospheric range (0 to 18 kPa; 85 kPa atmospheric pressure in Bozeman, MT, USA with 21% oxygen) relevant to bacterial growth conditions, we followed the procedure outlined by Mason *et al* (18). Alginate beads containing 90% w/v dispersed PFOB were prepared as described in section 2.2. The beads were placed into a 25 mL sample bottle immersed in DI water, and gases of variable oxygen content (100% air,

75% air/25% N_2, 50% air/50% N_2, 25% air/75% N_2, 100% N_2) were bubbled through the solution vigorously for 30 min. The area immediately above the liquid line was flooded with the appropriate gas, and the bottle was immediately sealed. The bottle was then loaded into a 25 mm dual tuning $^1H/^{19}F$ rf coil and bulk spin-lattice relaxation rate R_1 (=1/T_1) for the CF_3 peak was collected every 30 minutes. R_1 was measured spectroscopically using the Inversion Recovery (IR) method with the time domain sampled logarithmically at six points (TI = 25, 100, 300, 600, 1000, 3000, 5000 ms). Time-domain data was fit using Levenberg-Marquardt least-squares regression to a three-parameter mono-exponential formula governing the IR pulse sequence, yielding values for both signal intensity and R_1. Equilibrium was achieved within 1 hour, and therefore R_1 value at t = 1 hour was recorded. Three replicates were acquired for each point using different aliquots. Selective excitation of the CF_3 peak was accomplished using a 2 ms rf pulse. Oxygen concentration was reported in units of partial pressure in keeping with the convention of biomedical literature. Strictly speaking, the measurement denotes the gas-phase oxygen partial pressure that would be in equilibrium with the observed liquid-phase concentration. For example a pO_2 of 18 kPa indicates that the dissolved oxygen concentration in the sample corresponds to a gas-phase oxygen partial pressure of 18 kPa.

2.4 Packed bed column containing alginate beads

Immediately following alginate bead creation, excess calcium chloride solution was poured into a freshly autoclaved, 10 mm ID liquid chromatography column (Omnifit Labware) with 50 μm filters at both ends. Sterile beads were then wet-loaded into the column using a spatula. A single inoculated bead was loaded and moved into the center of the column at a height corresponding to the isocenter of the NMR coil. The column was filled with additional sterile beads and connected to a High Performance Liquid Chromatography Column (GE Healthcare; High Precision Pump P-500) with freshly autoclaved 1.9 mm ID Teflon tubing. The column outlet was connected to a waste collection bottle, forming an open flowthrough loop. The sample was then inserted into the coil and loaded into the magnet. Gradient cooling water was fixed at 22.8 ºC to ensure constant temperature in the magnet bore. A sterile solution containing full-strength TSB and 50 mM calcium chloride (to maintain alginate crosslinking) was flowed through the bed at a constant volumetric flowrate of 25 mL/hr (superficial velocity = 0.08 mm/s). The feed solution reservoir was maintained at ambient temperature (21 °C), and due to the extremely low flowrate, the solution was equilibrated with the 22.8 °C column by the time it entered the field of view. Immediately prior to this, laboratory air was bubbled through the feed solution to restore the dissolved oxygen lost during autoclaving. Bacterial air filters were attached to the feed bottle inlet and outlet tubing to maintain sterile conditions during bubbling. Oxygen distribution was tracked over the course of biofilm growth by continuous acquisition of 2D longitudinal R_1 maps which sampled three points along the inversion recovery curve (TI = 25, 1000, 3000 ms). A standard spin warp imaging sequence with IR preparation was used with acquisition parameters consisted of a 15 × 12 mm^2 field-of-view, 469 × 375 μm^2 spatial resolution, 8 ms echo time, 15 s repetition time to prevent T_1 weighting, slice thickness of 3 mm, 8 averages, and a total acquisition time of 192 min. Pixels were only assigned an R_1 if they achieved a threshold signal value of 10^5, corresponding to a signal-to-noise ratio of about 6, and the associated standard error of the measurement for the R_1 parameter fit was

below 15%. The T_1 error corresponds to a pO_2 error of +3.2/−2.3 kPa for the anoxic intercept and +6.4/−4.6 kPa for atmospheric conditions.

To investigate the well-documented phenomenon of infection persistence under antibiotic treatment, a subset of columns were subjected to a feed containing 50 μg/mL gentamicin (GEN), a broad-spectrum antibiotic that we found to completely inhibit planktonic *E. coli* growth when amended to the standard nutrient regimen (data not shown). Three experimental conditions were studied: a negative control with the entire protocol conducted in the absence of GEN treatment, a positive control with GEN administered throughout the experiment, and an experimental regimen wherein GEN administration began after about 20 hours of growth (at which point a substantial oxygen sink had developed), was continued for approximately 24 hours, and then was removed from the feed. Oxygen monitoring continued after removal of GEN from the feed reservoir.

2.5 Cell count experiments

Viable cell counts were measured at three different points in the packed bed experiment: immediately after bead creation (initial cell count), immediately before GEN exposure, and after 24 hours of GEN treatment. The initial cell count was carried out immediately after bead creation; ten sterile beads and ten inoculated beads were each dissolved in 10 mL of a 50 mM sodium citrate solution. Each was serially diluted to $1{:}10^6$ and 5 drops of 10 μL from each dilution were plated on tryptic soy agar. This was performed in triplicate for each dilution. Plates were incubated at 37 ºC for 6 to 8 hours until colonies were easily visible but well separated and counted.

It was discovered that over the course of the packed bed experiment, most colonies (or at least the fastest growing colonies) shed their RPF plasmid, making it impossible to identify the inoculated bead for cell counting. Thus for the later time points, an additional fluorescent tagging step was incorporated into the emulsion creation protocol to allow the inoculated beads to be distinguished. This was accomplished using the fluorescent tag PKH-26, which in addition to its uses for tagging cell membranes, is also known to tag the phosphatidylcholine surfactant used in the PFC emulsion (30). A PKH-26 Fluorescent Cell Linker kit was obtained from Sigma (MINI26). For these beads, PFOB and the surfactant were dissolved in water and emulsified in the absence of sodium alginate. The emulsion was separated into 2 aliquots (a 10mL and a 1 mL), and centrifuged at 4700 rpm for 4 minutes. The 10 mL emulsion was resuspended in DI water while the 1 mL aliquot was resuspended in the diluent C provided with the linker kit which optimizes PKH-26 binding. 10 μL of the ethanolic dye was dissolved in 0.25 mL of diluent, and this solution was mixed with the emulsion and mixed with gentle pipetting and shaking. The emulsion was incubated for 15 minutes to allow for binding, and then both emulsion aliquots were again centrifuged at 4700 rpm for 4 minutes and resuspended in DI water. 2% w/v sodium alginate were added to both and allowed to dissolve fully, and the 1 mL aliquot was inoculated as described above. Beads were then created from each as normal. The PKH-26 tagging step resulted in brightly fluorescent inoculated beads that were easily distinguishable with the naked eye, but otherwise identical to non-tagged beads.

The packed bed columns containing beads tagged with PKH-26 were used only for cell counting and were therefore operated outside the magnet but otherwise followed the same procedure. At the appropriate time point, the column was disconnected from the tubing and emptied out in a biological safety cabinet. The inoculated bead and 10 beads adjacent to the inoculated bead were dissolved in 1 mL and 10 mL of 50 mM sodium citrate, respectively. Plate counts for each were conducted as described above, with the PKH-26 tag allowing for identification of the inoculated bead. As excess PKH-26 was removed from the emulsion prior to bacterial inoculation by centrifugation and disposal of supernatant, we do not expect any unintended binding to cell membranes which could have influenced growth rate. Additionally, even if trace amounts of PKH-26 evaded removal during the centrifugation step, incorporation of PKH-26 into the cell membrane does not affect cell viability or behavior (31). Finally, because PKH-26 tagged beads were used only for cell counting and not for oxygen measurements, any potential influence of PKH-26 labeling on the oxygen sensitivity of emulsified PFOB did not affect results.

3. RESULTS

The emulsion of PFOB in water exhibited a strong sensitivity to changes in oxygen partial pressure (Figure 1) and due to the tight temperature tolerances provided by the NMR gradient cooling water (T = 22.8 ± 0.5 °C), the accuracy and precision of pO_2 measurements are not impacted by temperature uncertainty. This is reflected in the high fidelity of the pO_2 vs R_1 curve fit. The dependence of the CF_3 ^{19}F resonance on oxygen was found to be R_1 = 0.3517 (±0.0145) + 0.0194 (±0.0145)*pO_2(kPa), with error for slope and intercept representing 95% confidence. Converting pO_2 into gas-phase mass fraction to facilitate comparison with published data, we obtain R_1 = 0.3517 + 0.016543*pO_2(%). Mason et al. have investigated the relationship between oxygen concentration and R_1 for the same resonance peak at the same operating field strength (7 T) in a PFOB emulsion of slightly different makeup called Oxygent™ (32). Oxygent™, first developed by Alliance Pharmaceutical Corp, contains 3.6% w/v egg lecithin surfactant and 60% w/v PFOB (33). In contrast, the emulsion used in the current work contained a higher PFOB fraction (90% w/v) and used only a specific chemical component of egg lecithin (α-phosphatidylcholine) as the stabilizing surfactant rather than unprocessed lecithin itself. Nonetheless, Mason et al. reported a similar pO_2 sensitivity for the CF_3 peak of the Oxygent™ emulsion, with a general dependence of R_1 = 0.553 – 0.0059* T(°C) +0.023*pO_2(%) – 0.00019* T*pO_2. Evaluated at our operating temperature of 22.8 °C, the relationship becomes R_1 = 0.418 + 0.0187*pO_2(%), similar both in intercept and slope to the dependence reported here. It is unknown what accounts for the modest discrepancy between the two calibration curves but it may be related to the distinct chemical compositions of the two emulsions, due to differences in production (the manufacturing process of Oxygent™ remains proprietary), or due to the nonlinear response of R_1 to temperature (34).

In the absence of GEN (negative control), the column was characterized by an extended period of time (~8 hours) in which oxygen levels remained at saturation levels (Figure 2). In this phase, bacterial counts were low and the total oxygen consumption rate was small enough to be overwhelmed by the rate of oxygen replenishment due to flow. Around the 750–850 min mark, a modest oxygen sink developed and, due to the exponential growth of

the immobilized bacteria, rapidly grew in strength, with oxygen levels within the inoculated bead dropping to zero shortly after. The oxygen sink then spread through the rest of the column as *E. coli* colonies relocated to adjacent beads where oxygen was still available through bead contact points, rendering the entire column anoxic. Figure 3 presents the corresponding data for a representative column exposed to GEN. Following establishment of the biofilm (when a strong oxygen sink was evident), the standard TSB feed was replaced with an equivalent feed with the addition of 50 μg/mL GEN. This caused the oxygen sink to immediately become static; during the ~24 hours of administration, the oxygen sink neither expanded nor diminished. Following removal of GEN, the oxygen sink rapidly resumed its expansion. The behavior of the negative control column and two GEN columns are also evident in Figure 4, which presents the average oxygen value of the inoculated bead for the various experimental conditions over time.

In the positive control, GEN administration began at the start of the experiment and continued uninterrupted throughout (Figure 4). This condition resulted in no bacterial growth and the absence of an oxygen sink. In the experimental condition, the bacteria were allowed 20 hours of growth to establish a biofilm before GEN administration. Plate counts revealed that over this time period bacterial counts in the inoculated bead rose from the initial inoculum concentration of ~$\log_{10}$ 5.4 Colony Forming Units (CFU)/mL to about $\log_{10}$ 9.2 CFU/mL (Figure 5), while beads adjacent to the inoculated bead experienced a growth from 0 to $\log_{10}$ 4.4 CFU/mL ($p < 0.001$ and $p = 0.015$, respectively). After this point, in contrast to the rapid depletion of oxygen in the absence of antibiotic, the onset of GEN exposure coincided with a “freezing” of the oxygen sink, characterized by ongoing oxygen usage but a complete lack of sink spatial expansion. This forced steady state persisted throughout the 24 hour exposure period. Cell counts conducted after the GEN treatment regimen indicated that cell viability was unaffected, with an average log reduction of 0.23 for the inoculated bead and 0.09 for the adjacent beads, both statistically insignificant ($p = 0.13$ and $p = 0.32$, respectively), over the exposure window. Following GEN removal, the oxygen sink resumed its spread throughout the column, albeit at a slower rate than that which was observed for biofilms never exposed to the antibiotic, underscoring the difficulty that a well-established infectious biofilm presents for effective treatment.

4. DISCUSSION & CONCLUSIONS

As with other aminoglycosides, GEN targets the bacterial ribosome, interfering with protein synthesis, and exhibits dose-dependent bacteriostatic or bactericidal activity (35). Literature reports of *E. coli* susceptibility to GEN range significantly depending on strain, with a minimum inhibitory concentration ranging from 4 to 256 μg/mL (36). Minimum biofilm eradication concentration is typically (but not always) higher, ranging from 4 to >1024 μg/mL. The concentration used in the present study of 50 μg/mL, in the middle of this range, was found to completely inhibit planktonic growth (data not shown) but was insufficient to generate even a single log reduction in viable cell counts. These results are consistent with and enrich the long-standing observations *in vitro* and *in vivo* that aggressive antibiotic treatment of mature biofilms is often insufficient to eradicate bacterial respiration (37–39), even in cases where viable cell counts are affected, and that following cessation of antimicrobial therapy biofilms often regrow (40–42).

Traditional investigations of biofilm oxygen usage are typically conducted on steady state biofilms wherein oxygen penetration no longer changes with time, and studies examining the effect of antibiotic administration often infer continued oxygen utilization by identifying anoxic conditions at the biofilm base or by probing the one-dimensional oxygen profile, with the exact response of the oxygen sink to antibiotic challenge unknown. Here we have demonstrated the temporary bacteriostatic effect of a high dose of broad-spectrum antibiotic on a developing biofilm exhibiting a dynamic oxygen sink using a novel, MRI-based technique in real time. The method exploits the linear dependence of ^{19}F R_1 in PFCs on pO_2, permitting direct quantification of oxygen (43). We show that gentamicin administration to a model infection results in establishment of a pseudo-steady state wherein oxygen consumption continues but oxygen sink development is halted for an extended period of time (at least 21 hours for one experiment and at least 25 hours for the other). Further, we have demonstrated the advantages and unique benefits afforded by this approach by achieving oxygen concentration mapping entirely noninvasively for a model clinical biofilm in two spatial dimensions, providing comprehensive snapshots of transient oxygen profile that would be intractable with traditional oximetry methods. This method thus serves as a novel means to visualize the proliferation and dispersion of actively growing cells and to probe the interactions between oxygen gradients and chemical environment. The thorough oxygen distribution measurements provided by this technique may prove invaluable for further study of antibiotic efficacy and bacterial metabolism in biofilm systems that are more representative of real clinically-relevant biofilms, which are often characterized by non-planar geometry (44–46), porous structure (47), and the presence of flow (48; 49), and which may be inaccessible to conventional microelectrode approaches.

The technique for biofilm oximetry used in this work has several distinct advantages and disadvantages when compared to the traditional microelectrode approach. Fundamentally, the NMR phenomenon exhibits low signal-to-noise, with μ−MRI functionally constrained to a maximum resolution of about 10×10 μm^3/voxel due to diffusion and T_2 limitations and realistic resolution for ^{19}F NMR oximetry will be lower due to reduced ^{19}F signal density when the PFC is dispersed throughout the sample of interest. For applications that require resolution of an oxygen profile at the lengthscale of individual cell clusters (tens to hundreds of microns), ^{19}F NMR oximetry is impractical and traditional methods have the advantage. The same signal-to-noise limitation introduces modest variability into the R_1 fitting process, resulting in lower precision than the microelectrode. Finally, the technique requires access to a high-field NMR spectrometer, an expensive piece of equipment, and hardware access is a significant barrier to accessibility. The microelectrode, in contrast, is inexpensive, portable, and accurate, and is the superior option for data collection in the field. However, the noninvasive nature of NMR oximetry makes it an appealing option for systems where physical introduction of a needle is problematic. In *in vitro* applications, microelectrode insertion may alter intrinsic system behavior due to unintentional introduction of oxygen along the insertion path or alteration of local flow patterns (14; 50). In potential clinical applications, the microelectrode approach involves patient discomfort, particularly when oxygen mapping requires many separate measurements and therefore repeated, potentially painful insertion of the sensor. For such applications, NMR oximetry offers a painless alternative for evaluation of oxygen delivery in the clinic.

While the current study pioneers the use of ^{19}F NMR oximetry for oxygen mapping in an *in vitro* biofilm, there is potential for the technique to be translated into clinical measurement. Aqueous emulsions of PFOB exhibit both low toxicity and high stability in aqueous phases, and it thus may be possible to introduce the oxygen sensor into infected human tissue in a hospital setting via topical application. If the emulsion is able to permeate human tissue effectively, ^{19}F NMR could then be used to evaluate oxygen penetration into surface wounds. Due to the strong prognostic significance of oxygen delivery into infected tissue (12), this measurement could aid in determining treatment strategy. NMR analysis could be accomplished using a surface NMR tool such as the NMR-MOUSE (51). The NMR-MOUSE is a permanent electromagnet that generates a B_o magnetic field in the sample it is placed against. It is also portable and relatively inexpensive, making it a feasible option for healthcare providers.

ACKNOWLEDGEMENTS

The authors wish to thank Kayla Keepseagle and Betsey Pitts for assistance with bacterial culturing, and Mike Franklin for providing bacteria. This work was funded by the National Institutes of Health award R01GM109452. JDS and SLC acknowledge equipment funding from the Murdock Charitable Trust and the National Science Foundation Major Research Instrumentation Program.

References

[1]. Stewart PS, and Franklin MJ Physiological heterogeneity in biofilms. Nature Reviews Microbiology 2008; 6: 199–210. [PubMed: 18264116]

[2]. Costerton JW, Lewandowski Z, Caldwell DE, Korber DR, and Lappin-Scott HM Microbial biofilms. Annu Rev Microbiol 1995; 49: 711–745. [PubMed: 8561477]

[3]. Prigent-Combaret C, Vidal O, Dorel C, and Lejeune P Abiotic surface sensing and biofilm-dependent regulation of gene expression in Escherichia coli. J Bacteriol 1999; 181: 5993–6002. [PubMed: 10498711]

[4]. Schobert M, and Tielen P Contribution of oxygen-limiting conditions to persistent infection of Pseudomonas aeruginosa. Future Microbiol 2010; 5: 603–621. [PubMed: 20353301]

[5]. Stewart PS, Zhang T, Xu R, Pitts B, Walters MC, Roe F, Kikhney J, and Moter A Reaction–diffusion theory explains hypoxia and heterogeneous growth within microbial biofilms associated with chronic infections. npj Biofilms and Microbiomes 2016; 2: 16012. [PubMed: 28721248]

[6]. Worlitzsch D, Tarran R, Ulrich M, Schwab U, Cekici A, Meyer KC, Birrer P, Bellon G, Berger J, and Weiss T Effects of reduced mucus oxygen concentration in airway Pseudomonas infections of cystic fibrosis patients. The Journal of clinical investigation 2002; 109: 317–325. [PubMed: 11827991]

[7]. Cowley ES, Kopf SH, LaRiviere A, Ziebis W, and Newman DK Pediatric cystic fibrosis sputum can be chemically dynamic, anoxic, and extremely reduced due to hydrogen sulfide formation. MBio 2015; 6: e00767–00715. [PubMed: 26220964]

[8]. Kolpen M, Hansen CR, Bjarnsholt T, Moser C, Christensen LD, van Gennip M, Ciofu O, Mandsberg L, Kharazmi A, and Döring G Polymorphonuclear leukocytes consume oxygen in sputum from chronic Pseudomonas aeruginosa pneumonia in cystic fibrosis. Thorax 2010; 65: 57–62. [PubMed: 19846469]

[9]. Borriello G, Werner E, Roe F, Kim AM, Ehrlich GD, and Stewart PS Oxygen limitation contributes to antibiotic tolerance of Pseudomonas aeruginosa in biofilms. Antimicrob Agents Chemother 2004; 48: 2659–2664. [PubMed: 15215123]

[10]. Kolpen M, Lerche CJ, Kragh KN, Sams T, Koren K, Jensen AS, Line L, Bjarnsholt T, Ciofu O, and Moser C Hyperbaric oxygen sensitizes anoxic Pseudomonas aeruginosa biofilm to ciprofloxacin. Antimicrob Agents Chemother 2017; 61: 1–9.

[11]. Jesaitis AJ, Franklin MJ, Berglund D, Sasaki M, Lord CI, Bleazard JB, Duffy JE, Beyenal H, and Lewandowski Z Compromised host defense on Pseudomonas aeruginosa biofilms: Characterization of neutrophil and biofilm interactions. J Immunol 2003; 171: 4329–4339. [PubMed: 14530358]

[12]. Schreml S, Szeimies RM, Prantl L, Karrer S, Landthaler M, and Babilas P Oxygen in acute and chronic wound healing. Br J Dermatol 2010; 163: 257–268. [PubMed: 20394633]

[13]. Ueno T, Omi T, Uchida E, Yokota H, and Kawana S Evaluation of hyperbaric oxygen therapy for chronic wounds. Journal of Nippon Medical School 2014; 81: 4–11. [PubMed: 24614389]

[14]. Davies PW, and Brink F Microelectrodes for measuring local oxygen tension in animal tissues. Rev Sci Instrum 1942; 13: 524–533.

[15]. Zhao D, Jiang L, and Mason RP (2004). Measuring changes in tumor oxygenation. In Methods Enzymol (Elsevier), pp. 378–418.

[16]. Eidelberg D, Johnson G, Barnes D, Tofts PS, Delpy D, Plummer D, and McDonald WI ^{19}F NMR imaging of blood oxygenation in the brain. Magn Reson Med 1988; 6: 344–352. [PubMed: 3362067]

[17]. Liu S, Shah SJ, Wilmes LJ, Feiner J, Kodibagkar VD, Wendland MF, Mason RP, Hylton N, Hopf HW, and Rollins MD Quantitative tissue oxygen measurement in multiple organs using 19F MRI in a rat model. Magn Reson Med 2011; 66: 1722–1730. [PubMed: 21688315]

[18]. Mason RP, Rodbumrung W, and Antich PP Hexafluorobenzene: A sensitive F-19 NMR indicator of tumor oxygenation. NMR Biomed 1996; 9: 125–134. [PubMed: 8892399]

[19]. Nöth U, Rodrigues LM, Robinson SP, Jork A, Zimmermann U, Newell B, and Griffiths JR In vivo determination of tumor oxygenation during growth and in response to carbogen breathing using 15C5-loaded alginate capsules as fluorine-19 magnetic resonance imaging oxygen sensors. International Journal of Radiation Oncology• Biology• Physics 2004; 60: 909–919.

[20]. Shukla HP, Mason RP, Bansal N, and Antich PP Regional myocardial oxygen tension: 19F MRI of sequestered perfluorocarbon. Magn Reson Med 1996; 35: 827–833. [PubMed: 8744009]

[21]. Barker BR, Mason RP, Bansal N, and Peshock RM Oxygen tension mapping with F-19 echo-planar MR imaging of sequestered perfluorocarbon. J Magn Reson Imaging 1994; 4: 595–602. [PubMed: 7949687]

[22]. Tran HT, Guo Q, Schumacher DJ, Buxton RB, and Mattrey RF 19F chemical shift imaging technique to measure intracellular pO2 in vivo using perflubron. Acad Radiol 1995; 2: 756–761. [PubMed: 9419636]

[23]. Guo Q, Mattrey R, Guclu C, Buxton R, and Nalcioglu O Monitoring of pO2 by spin-spin relaxation rate 1/T2 of 19F in a rabbit abscess model. Artificial Cells, Blood Substitutes, and Biotechnology 1994; 22: 1449–1454.

[24]. Simkins JW, Stewart PS, and Seymour JD Spatiotemporal mapping of oxygen in a microbially-impacted packed bed using 19 F Nuclear magnetic resonance oximetry. J Magn Reson 2018; 293: 123–133. [PubMed: 29940412]

[25]. Smidsrød O, and Skja G Alginate as immobilization matrix for cells. Trends Biotechnol 1990; 8: 71–78. [PubMed: 1366500]

[26]. Cheetham PS, Blunt KW, and Bocke C Physical studies on cell immobilization using calcium alginate gels. Biotechnol Bioeng 1979; 21: 2155–2168.

[27]. Pabst B, Pitts B, Lauchnor E, and Stewart PS Gel-entrapped Staphylococcus aureus bacteria as models of biofilm infection exhibit growth in dense aggregates, oxygen limitation, antibiotic tolerance, and heterogeneous gene expression. Antimicrob Agents Chemother 2016; 60: 6294–6301. [PubMed: 27503656]

[28]. Sønderholm M, Koren K, Wangpraseurt D, Jensen PØ, Kolpen M, Kragh KN, Bjarnsholt T, and Kühl M Tools for studying growth patterns and chemical dynamics of aggregated Pseudomonas aeruginosa exposed to different electron acceptors in an alginate bead model. NPJ biofilms and microbiomes 2018; 4: 3. [PubMed: 29479470]

[29]. Sønderholm M, Kragh KN, Koren K, Jakobsen TH, Darch SE, Alhede M, Jensen PØ, Whiteley M, Kühl M, and Bjarnsholt T Pseudomonas aeruginosa aggregate formation in an alginate bead model system exhibits in vivo-like characteristics. Appl Environ Microbiol 2017; 83: e00113–00117. [PubMed: 28258141]

[30]. Smith D, Kornbrust E, and Lane T Phagocytosis of a fluorescently labeled perflubron emulsion by a human monocyte cell line. Artificial Cells, Blood Substitutes, and Biotechnology 1994; 22: 1215–1221.

[31]. Slezak SE, and Horan PK Fluorescent in vivo tracking of hematopoietic cells. Part I. Technical considerations. Blood 1989; 74: 2172–2177. [PubMed: 2804356]

[32]. Mason RP, Shukla H, and Antich PP Oxygent™; A Novel Probe of Tissue Oxygen Tension. Biomaterials, Artificial Cells and Immobilization Biotechnology 1992; 20: 929–932.

[33]. Keipert PE Use of Oxygent™, a perfluorochemical-based oxygen carrier, as an alternative to intraoperative blood transfusion. Artificial Cells, Blood Substitutes, and Biotechnology 1995; 23: 381–394.

[34]. Shukla HP, Mason RP, Woessner DE, and Antich PP A Comparison of Three Commercial Perfluorocarbon Emulsions as High-Field 19F NMR Probes of Oxygen Tension and Temperature. Journal of Magnetic Resonance, Series B 1995; 106: 131–141.

[35]. Yoshizawa S, Fourmy D, and Puglisi JD Structural origins of gentamicin antibiotic action. The EMBO journal 1998; 17: 6437–6448. [PubMed: 9822590]

[36]. Olson ME, Ceri H, Morck DW, Buret AG, and Read RR Biofilm bacteria: formation and comparative susceptibility to antibiotics. Can J Vet Res 2002; 66: 86. [PubMed: 11989739]

[37]. von Ohle C, Gieseke A, Nistico L, Decker EM, and Stoodley P Real-time microsensor measurement of local metabolic activities in ex vivo dental biofilms exposed to sucrose and treated with chlorhexidine. Appl Environ Microbiol 2010; 76: 2326–2334. [PubMed: 20118374]

[38]. Kiamco MM, Atci E, Mohamed A, Call DR, and Beyenal H Hyperosmotic agents and antibiotics affect dissolved oxygen and pH concentration gradients in Staphylococcus aureus biofilms. Appl Environ Microbiol 2017: AEM. 02783–02716.

[39]. Kiamco MM, Atci E, Khan QF, Mohamed A, Renslow RS, Abu-Lail N, Fransson BA, Call DR, and Beyenal H Vancomycin and maltodextrin affect structure and activity of Staphylococcus aureus biofilms. Biotechnol Bioeng 2015; 112: 2562–2570. [PubMed: 26084588]

[40]. Haagensen J, Verotta D, Huang L, Engel J, Spormann AM, and Yang K Spatiotemporal pharmacodynamics of meropenem-and tobramycin-treated Pseudomonas aeruginosa biofilms. J Antimicrob Chemother 2017; 72: 3357–3365. [PubMed: 28961810]

[41]. Ito A, Taniuchi A, May T, Kawata K, and Okabe S Increased antibiotic resistance of Escherichia coli in mature biofilms. Appl Environ Microbiol 2009; 75: 4093–4100. [PubMed: 19376922]

[42]. Anwar H, Strap J, Chen K, and Costerton J Dynamic interactions of biofilms of mucoid Pseudomonas aeruginosa with tobramycin and piperacillin. Antimicrob Agents Chemother 1992; 36: 1208–1214. [PubMed: 1416820]

[43]. Kodibagkar VD, Wang X, and Mason RP Physical principles of quantitative nuclear magnetic resonance oximetry. Front Biosci 2008; 13: 1371–1384. [PubMed: 17981636]

[44]. Klapper I Effect of heterogeneous structure in mechanically unstressed biofilms on overall growth. Bull Math Biol 2004; 66: 809–824. [PubMed: 15210320]

[45]. Bjarnsholt T, Alhede M, Alhede M, Eickhardt-Sørensen SR, Moser C, Kühl M, Jensen PØ, and Høiby N The in vivo biofilm. Trends Microbiol 2013; 21: 466–474. [PubMed: 23827084]

[46]. Wu Y, Klapper I, and Stewart PS Hypoxia arising from concerted oxygen consumption by neutrophils and microorganisms in biofilms. Pathogens and disease 2018; 76: fty043.

[47]. Høiby N Understanding bacterial biofilms in patients with cystic fibrosis: current and innovative approaches to potential therapies. Journal of Cystic Fibrosis 2002; 1: 249–254. [PubMed: 15463822]

[48]. Grubb SE, Murdoch C, Sudbery PE, Saville SP, Lopez-Ribot JL, and Thornhill MH Adhesion of Candida albicans to endothelial cells under physiological conditions of flow. Infect Immun 2009; 77: 3872–3878. [PubMed: 19581400]

[49]. Stewart PS Biophysics of biofilm infection. Pathogens and disease 2014; 70: 212–218. [PubMed: 24376149]

[50]. Silver IA (1973). Problems in the investigation of tissue oxygen microenvironment. In Chemical Engineering in Medicine (American Chemical Society), pp. 343–352.

[51]. Eidmann G, Savelsberg R, Blümler P, and Blümich B The NMR MOUSE, a mobile universal surface explorer. J Magn Reson 1996; 122: 104–109.

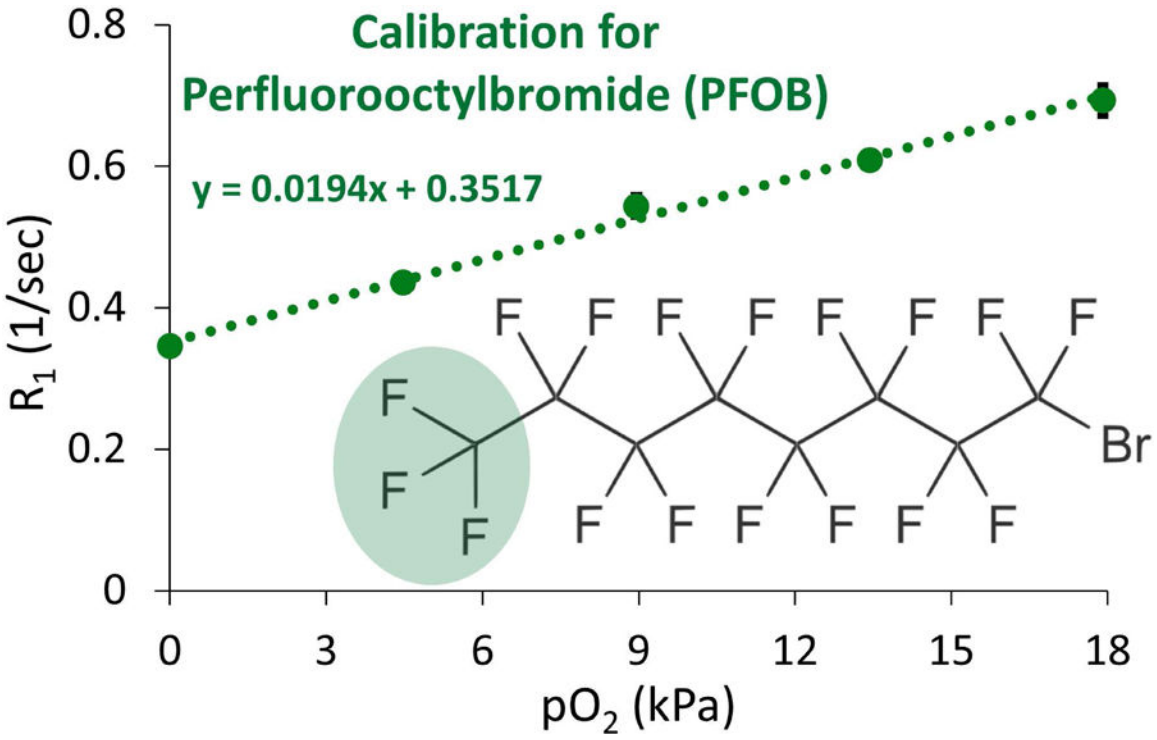

Figure 1.

Calibration curve relating the response of spin-lattice relaxation R_1 to pO_2 for PFOB encapsulated in alginate beads at 7 T and 22.8 °C. All points were measured in triplicate, and error bars denote standard deviation. Where error bars are not apparent, standard deviation is smaller than the marker size. The resonance peak chosen to measure R_1 for PFOB (CF_3 group) is highlighted in green.

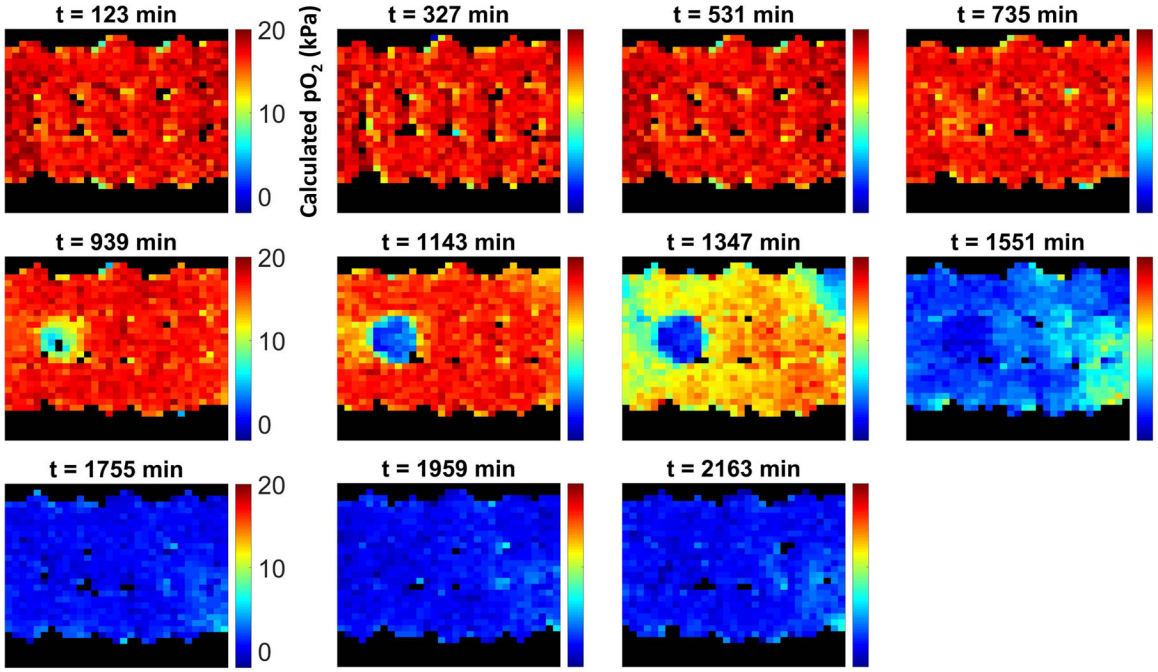

Figure 2.

Longitudinal map of calculated pO_2 values over time within a packed bed column containing a single alginate bead inoculated with *E. coli*.

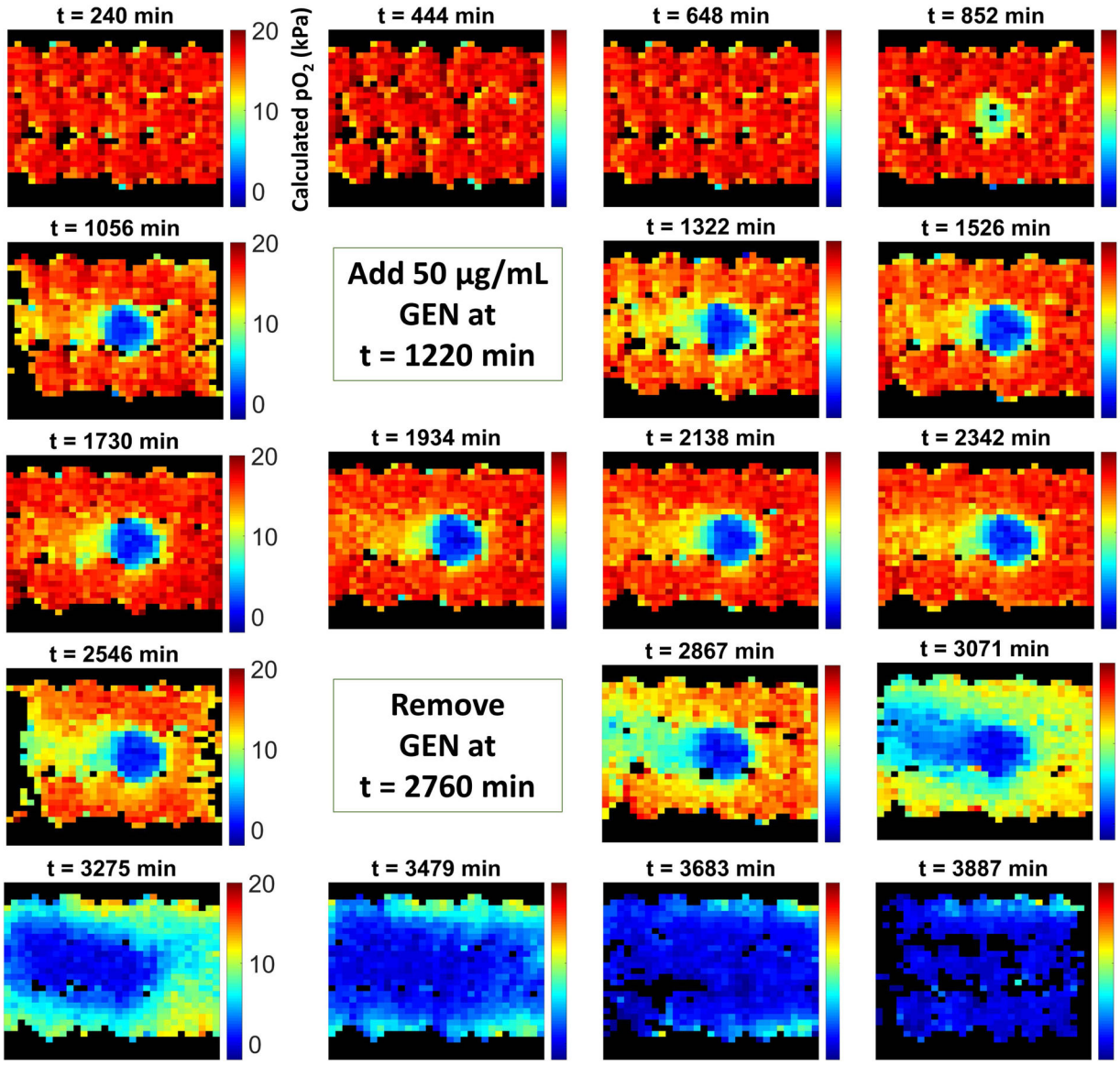

Figure 3.

Longitudinal map of calculated pO_2 values for a packed bed column exposed to a 24 hour treatment of 50 µg/mL gentamicin, a broad-spectrum antibiotic, following development of the oxygen sink due to *E. coli* growth.

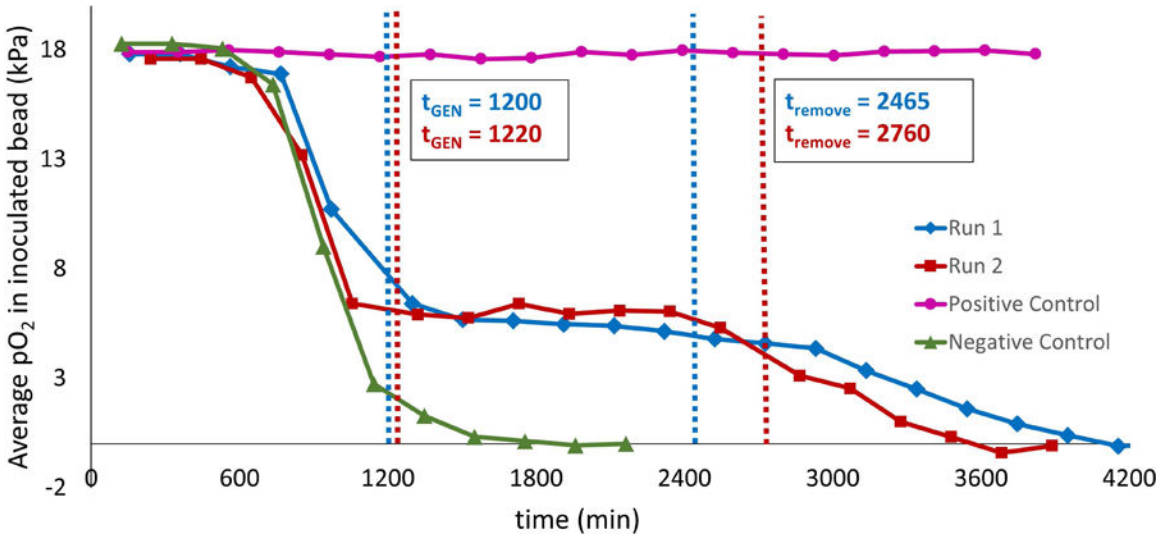

Figure 4.

Average calculated pO_2 in inoculated bead for negative control (no GEN treatment; green triangles), positive control (GEN treated throughout experiment; pink circles), and experimental regimen (GEN treated from t = 20 hours to t = 44 hours; red squares and blue diamonds).

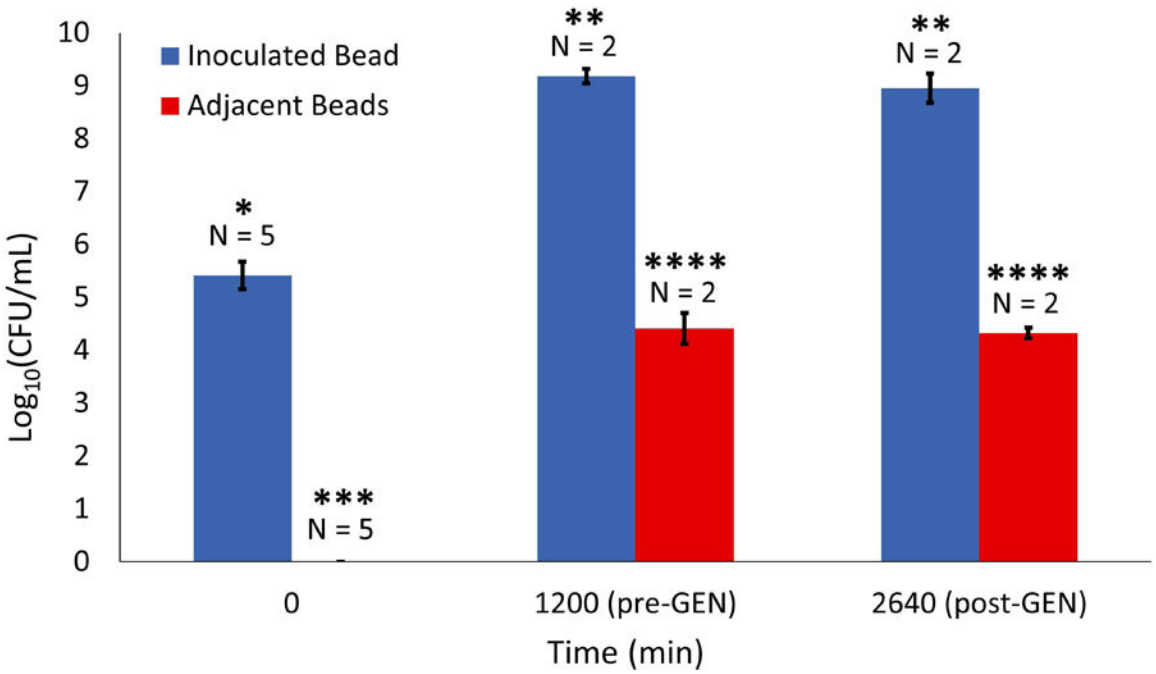

Figure 5.

Viable cell counts for inoculated bead (blue) and adjacent beads (red) at beginning of experiment, immediately prior to GEN treatment, and after 24 hours of GEN treatment. Error bars represent standard deviation and asterisks denote significant differences.